Precursor ionization and propagation velocity of a laser-absorption wave in 1.053 and 10.6 μm wavelengths laser radiation

Kohei Shimamura, *Member, IEEE*, Kimiya Komurasaki, Joseph A. Ofosu, and Hiroyuki Koizumi

***Abstract*—A propagation model of a laser-absorption wave was proposed and validated using the measured propagation velocity. The model describes the propagation mechanism in terms of avalanche ionization through an inverse Bremsstrahlung process and photo-ionization by UV radiation from bulk plasma behind the wave. Using plasma spectroscopy, the electron temperature and density at the head of laser-absorption wave were estimated as 2 eV and (1.5–2.6) × 10^{24} m^{-3}, respectively at 10.6 μm laser wavelength and 5 eV and (2.6–3.3) × 10^{24} m^{-3} at 1.05 μm when the laser intensity was near the laser-supported detonation threshold in the air and argon atmosphere. Using the measured plasma properties, we estimated UV photon flux radiated by the Bremsstrahlung which contributes the photoionization ahead of the laser-absorption wave. The resulting propagation velocity of the laser-absorption wave was 10^3 m/s, which showed good agreement with the velocity measured using a high-speed camera.**

***Index Terms*—Laser-induced plasma, laser propulsion, plasma measurement, shock wave.**

I. Introduction

At a certain laser intensity, a shock front (S-front) and an ionization-wave front (I-front) travel at a supersonic velocity in the laser light channel along the direction opposite that of the beam incidence. Discovered by Ramsden[1] and Raizer[2] using a Q-spoiled ruby laser, this phenomenon has been recognized as optical detonation. At laser intensities S greater than 10^7 W/cm^2, the incident laser energy is absorbed at the shock front to create a laser-supported detonation (LSD) wave.[3] In the LSD regime, a laser absorption layer propagating with the shock wave corresponding to a combustion layer in chemical detonation. As the laser intensity on the LSD wave decreases, the I-front is left behind the S-front. The remaining plasma is heated in an isobaric condition. The absorption regime invariably shifts from LSD to laser-supported combustion during laser irradiation. Several studies have characterized the laser-absorption waves driven by a point-focusing laser beam experimentally under various focusing f-numbers, total laser energy, and ambient pressures using shadowgraph visualization to investigate the fundamental theory of laser propulsion.[4]-[6]

The propagation process of the laser-absorption wave was investigated by Raizer in the 1970s.[7] The laser-absorption wave velocity was introduced by analysis of one-dimensional steady-state flow with heat interaction. The shock wave is sufficiently strong that the shocked heated gas is sufficiently hot to begin absorbing the laser irradiation. This is an analog of the chemical detonation-wave that can be viewed as a shock followed by a strong deflagration. However, the velocity given by a Chapman–Jouguet relation does not agree with the measurements.[8],[9] Raizer suggested that some non-hydrodynamic ionization mechanism is more dominant than the shock wave, from the analog of overdriven detonation. Overdriven detonation is categorized into strong and weak detonation, and a pressure-specific volume (p-V) diagram can describe these situations with a Hugoniot curve, a Rayleigh line, and a shock adiabatic curve. Strong-overdriven detonation occurs in the presence of additional external agency acting on the gas, such as a supersonic piston. However, it is difficult to show a von-Neumann spike on the shock adiabatic curve because there is no piston in this case. The weakly overdriven detonation wave is a suitable situation for the laser absorption wave because the laser-absorption occurs ahead of and after the shock wave. The pressure increases continuously from the preionized layer to the back surface of the laser absorption layer.[7] This detonation mode is difficult to explain simply in terms of the hydrodynamics relations.

Some causative relations between precursor ionization and I-front propagation were found in a previous study with a two-wave Mach–Zehnder interferometer.[10] During the laser-absorption process, a distribution of electron density was observed ahead of the shock wave. Laser absorption occurs from the preionization layer before shock heating. Results

Manuscript received October 31, 2013; revised January 10, 2014; accepted January 28, 2014. Date of publication Oct. xx, 2014; date of current version xxx xx, 2014. This work was supported in part by a Grant-in-Aid for Scientific Research (a), No. 23246145, supported by the Ministry of Education, Culture, Sports, Science and Technology (MEXT), Japan, and by a Grant-in-Aid for JSPS fellows, No.25203, sponsored by Japan Society for the Promotion of Science (JSPS), Japan.

K. Shimamura was with the Department of Advanced Energy, University of Tokyo. He is now with the Department of Engineering Mechanics and Energy, University of Tsukuba, 1-1-1 Tennodai, Tsukuba, Ibaraki 305-8573, Japan (e-mail: kohei.shimamura@gmail.com)

K. Komurasaki and J. A. Ofosu are with the Department of Advanced Energy, University of Tokyo, 5-1-5 Kashiwanoha, Kashiwa, Chiba, 277-8561, Japan (e-mail: komurasaki@k.u-tokyo.ac.jp, joseph@al.t.u-tokyo.ac.jp).

H. Koizumi is with the Research Center for Advanced Science and Technology, University of Tokyo, 4-6-1, Komaba, Meguro, Tokyo, 153-8904, Japan (e-mail: koizumi@al.t.u-tokyo.ac.jp).

Digital Object Identifier….

reveal that the contribution of shock heating is less important than that of preionization. The ionization event ahead of the shock wave regulates propagation of the laser-absorption wave. Similar phenomena have been observed in gaseous electronic discharge. The filamentary plasma patterns induced by high-power microwave beam were observed.[11],[12] The advancement of the streamer head, of which the velocity tends to achieve 10^7–10^9 m/s, was explained using the relation between the product of seed electrons and the avalanche ionization.[13] Consequently, it might be possible to elucidate the I-front velocity of the laser-absorption wave by the gaseous discharge theory.

This study was conducted to elucidate the propagation of laser-absorption wave in the weak overdriven detonation mode using the gaseous discharge theory. Optical emission spectroscopy was applied to bulk plasma behind the shock wave to evaluate the UV radiation because the degree of ionization in the preionization layer is so small that it is difficult to obtain the spectra in a short period. To compare the laser-wavelength and gaseous form, a Nd:Glass laser (λ = 1.05 μm) and a TEA CO_2 laser (λ = 10.6 μm) were used with Argon and air contained separately in the test chamber. The model was verified using results of the shadowgraph experiment.

II. Experimental Arrangement and Methods

A. Lasers and Focusing Optics

A Nd:glass laser was used. The pulse durations were approximately 0.30 μs and 0.45 μs, during which 80% and 90% of all pulse energy were irradiated, respectively. Pulse energy E_i was measured using an energy meter. The subsequent shot-to-shot pulse energy fluctuations were kept below 5% throughout experimentation. Its single pulse energy is up to 2 J, with a 10-mm diameter of the circular cross-section. A multi-transverse mode was top-hat shaped.[14] A lens with 62.7 mm focal length focused the laser beam with no target. Temporal laser power profiles are presented in Fig. 1(a). The LSD termination time t_{term} and the threshold laser intensity for its regime transition in E_i = 1 J are, respectively, 0.30 μs and 175 MW/cm^2.[14] A TEA CO_2 pulse laser was used. It had pulse duration of approximately 3 μs, during which 95% of E_i was irradiated. Variation of E_i was less than ±5% pulse-to-pulse. The laser beam has a 30×30 mm square cross section. Its effective radius and single pulse energy were, respectively, 34 mm and 7 J. The distribution of the laser energy density for lateral and vertical direction were, respectively, flat topped and approximately Gaussian.[4] An off-axis parabolic mirror with 35 mm focal length focused the laser beam. Temporal laser power profiles are presented in Fig. 1(b): The initial ambient gas density was 2.53×10^{25} m^{-3}. The laser pulse shape and the air conditions are identical to those used in our previous study.[4]–[6].

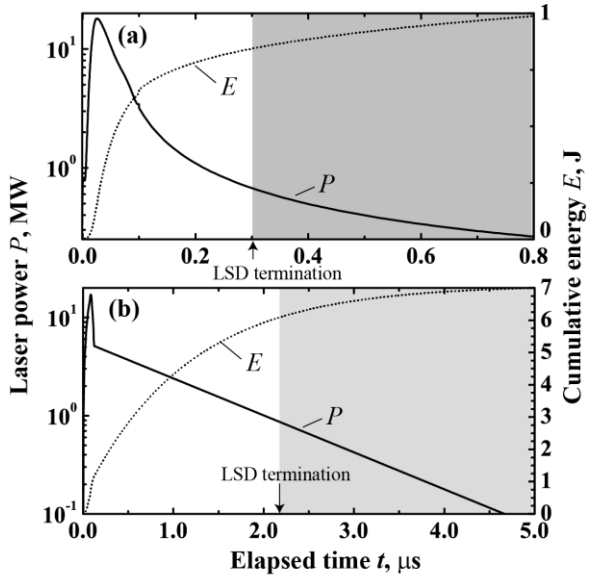

Fig. 1. Laser pulse shape and its cumulative energy for Nd:Glass laser (a) (E_i = 1 J) and TEA CO_2 laser (b) (E_i = 7 J).

B. Emission Spectroscopy and Laser shadowgraphy

The gates of the spectrometer and laser operations were controlled using a pulsed-delay generator (DG535; Stanford Research Systems Inc.), which first receives a trigger signal from the lasers. After adding a delay, it triggers the camera and the shutter controller, as presented in Fig. 2. Irradiation of the plasma was corrected using a mirror, lenses (solid angle: π/18), and an optical fiber connected to an echelle spectrometer (Aryelle 200; LaserTechnik GmbH, Berlin) with an ICCD camera (resolution 1,024 × 1,024 pixels, iStar 734-18-F-03; Andor Technology), of which the spectral resolution $\lambda/\Delta\lambda$ is 8,000 between wavelengths of 190 nm and 900 nm. In the 10.6 μm laser experiment, the spectrometer shutter exposure time was 0.20 μs. For the 1 μm laser experiment, all data were taken

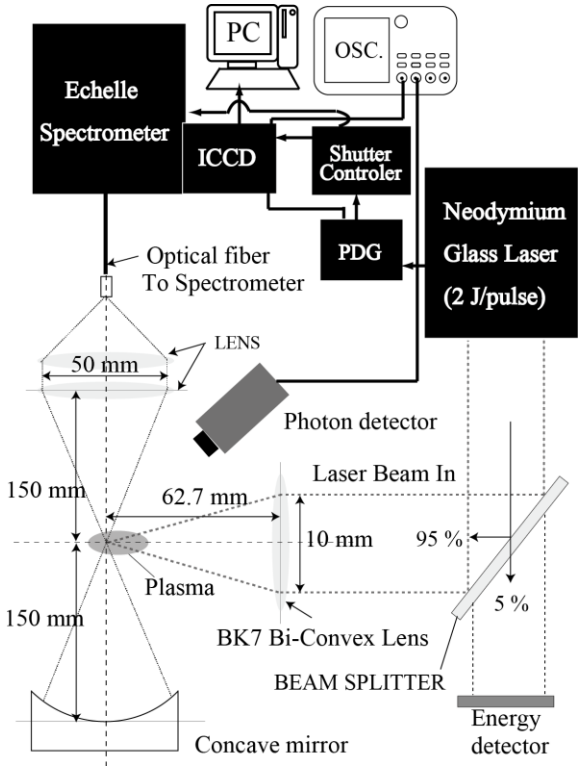

Fig. 2. Schematic of emission spectroscopy with Nd:Glass laser.

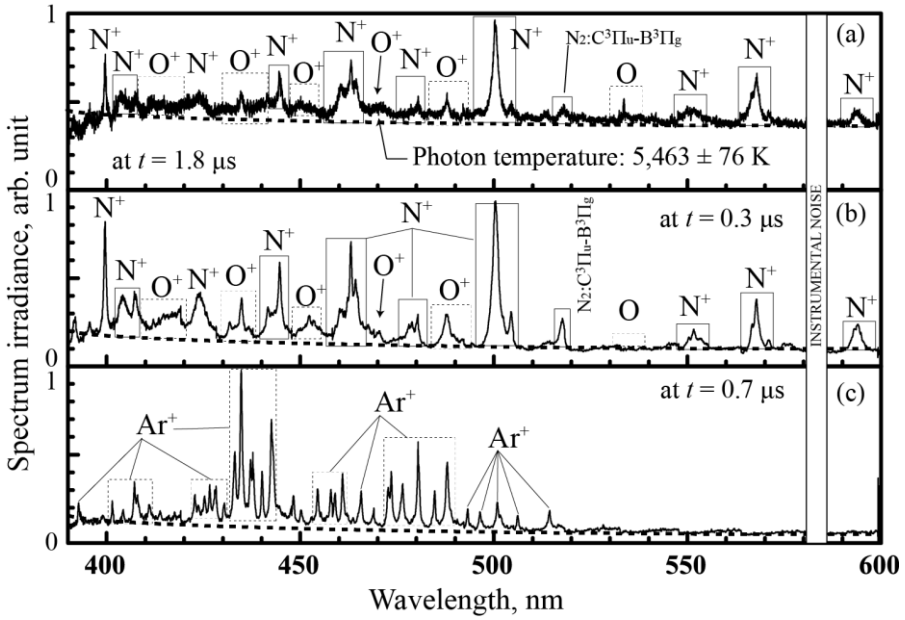

Fig. 3. Spectra from laser-induced plasma using (a) the CO_2 laser, (b) the Nd:Glass laser in air, and (c) the Nd:Glass laser in argon.

during the 0.05 μs exposure time. One datum was taken in 50 experimental operations. The experiment was repeated several times to confirm its reproducibility. The wavelength and sensitivity were calibrated, respectively, using a Hg-lamp and a halogen lamp.

A laser-shadowgraph method was used in the same manner as that described for previous studies.[4],[14] A 532 nm DPSS laser (MGL-H-532; Changchun New Industries Optoelectronics Technology Co. Ltd.) with 1.4 W output power was used as a probe light. It projects the shadow of the laser-induced plasma and the shock wave on a high-speed ICCD camera (resolution 520×520 pixels, Ultra 8; DRS Technologies Inc.) that can take eight frames in each operation at the minimum exposure time of 10 ns. This ICCD was also operated by the pulse-delay generator. One image was taken in one experimental operation. Displacement of the I-front was determined by averaging five data samples. Temporal and spatial resolutions were, respectively, 30 ns and 10^{-5} m.

III. Determination of Plasma Temperature and Density

Typical emission spectra from the bulk plasma behind the shock wave are depicted in Fig. 3. The time elapsed after the laser irradiation is indicated in each spectrum. Several lines of N II and continuous spectral line are apparent between wavelengths of 400–600 nm for Figs. 3(a) and 3(b). In Fig. 3(c), Ar II spectra were observed. An instrumental noise caused by characteristics of the echelle spectrometer was excluded from these spectra (from λ = 580–585 nm). A Planck function was used for subtracting the continuum radiation, of which the corresponding photon temperature T_{hv} was 5–8×10^3 K.[15] This temperature is much lower than the electronic excitation temperature (approx. 10^4 K) estimated by the Boltzmann plot. The peak of electron temperature and density distribution locates at the head of LSD wave.[10] The point of spectroscopic measurement was chosen as the highest intensity spot. Therefore, this point was observed at the front of LSD wave.

Figure 4 shows the Stark broadening profile of N II line and electron number density n_e deduced using the lines at λ = 399.5 nm and 504 nm. The spectral lines were fitted with a pseudo-Voigt function, as the approximation of the Voigt line shape by the sum of a Lorentzian and Gauss function.[16] For the laser plasma, other broadening mechanisms contributing to the Lorentzian profile, such as pressure broadening and natural broadening, are negligibly small in comparison with the Stark broadening. Generally, the FWHM of natural broadening is smaller than that of pressure broadening, of which the mechanism is generally unimportant in highly ionized plasmas such as laser-induced plasma.[17] In this case, instrumental line broadening was also negligibly small. The FWHM of a Lorentzian width $\Delta\lambda_L$ (nm) is a function of n_e and the electron-impact half width W (nm), $n_e = 5.0\times10^{21}\,\Delta\lambda_L / W(T_e)$. [18] As presented in Fig. 5, n_e was of the order of (1.5–3.9) × 10^{24} m^{-3} for 1.05 μm and 10.6 μm laser-wavelength. In the following figures, error bars respectively represent a standard deviation of

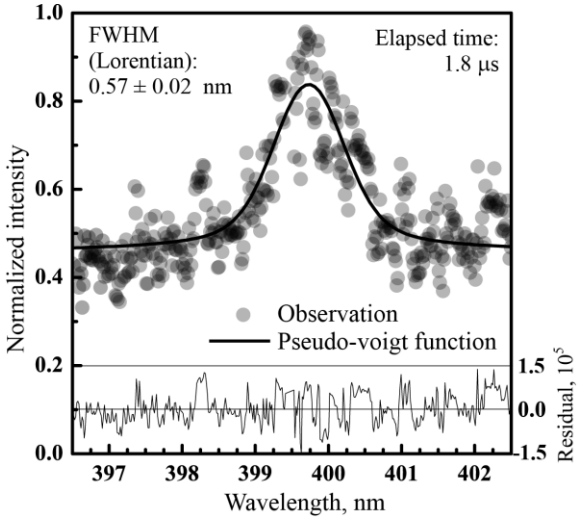

Fig. 4. Results of spectral line fitting with a pseudo-Voigt function at 1.8 μs.

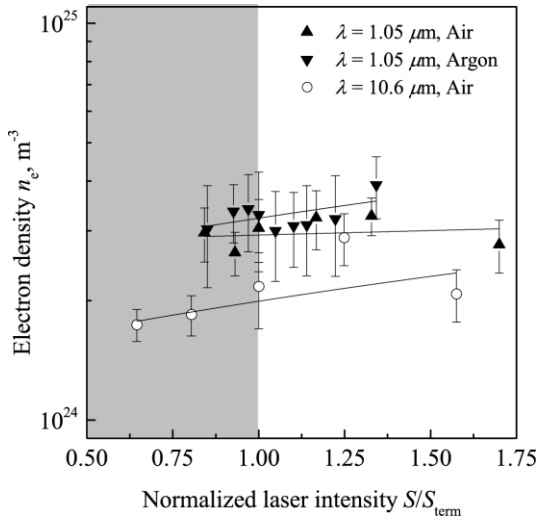

Fig. 5. Variation of n_e as a function of normalized laser intensity in the glass and CO_2 laser experiments. Symbols ▲,▼ and ● respectively represent n_e in Air (1 μm), Argon (1 μm), and Air (10.6 μm).

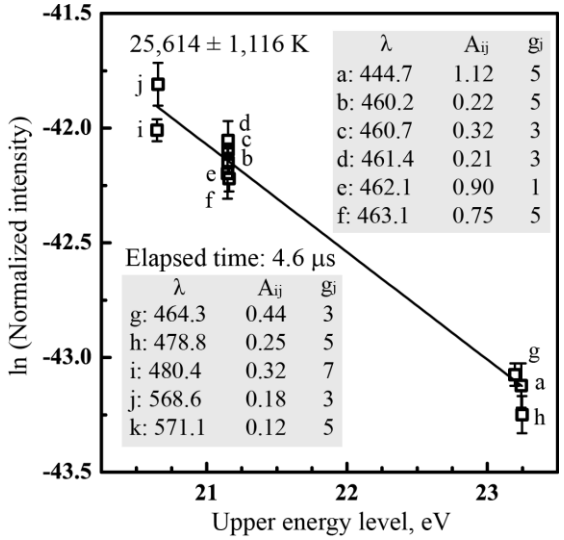

Fig. 6. Examples of Boltzmann plots of the observed emission lines of N II.[18] (Using CO_2 laser).

five measurements. Figure 6 shows a Boltzmann plot drawn using the NIST database [19] along with the estimate T_{ex} and physical constants used. In the 10.6 μm laser experiment, the observed emission lines at high laser intensities were broadened considerably such that it was impossible to distinguish the spectra and to use the fitting analysis. A possible means is to use the Stark broadening effect of N II 399 and 504 nm lines for T_e estimation: The impact parameter is a function of T_e. If $\Delta\lambda_L$ is known, then T_e can be determined using the following formula.

$$\frac{\Delta\lambda_{399}}{\Delta\lambda_{504}} = \frac{W_{504}(T_e)}{W_{399}(T_e)} = \frac{a + bT_e + cT_e^2}{a' + b'T_e + c'T_e^2} \quad (1)$$

Therein, W_{399} (T_e) and W_{504} (T_e), respectively represent impact parameters for 399 nm and 504 nm. *a, b, c, a', b',* and *c'* are the linear interpolation coefficients. In this study, temperature verification was achieved by comparison with the

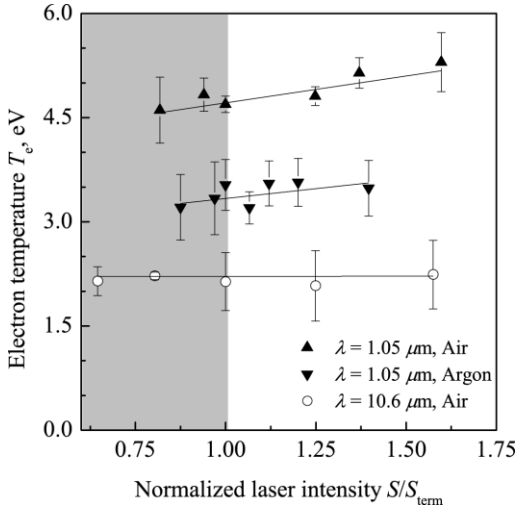

Fig. 7. Variation of electron temperature as a function of normalized laser intensity with fitted solid lines.

Boltzmann plot during 3–5 μs. Consequently, T_e using the Stark effect showed good agreement with T_{ex} using a Boltzmann plot. Figure 7 presents estimated temperatures of the bulk plasma behind the shock wave. T_e = 2 eV for 10.6 μm laser wavelength and T_e = 5 eV for 1.05 μm laser wavelength were observed.

IV. I-FRONT PROPAGATION IN TERMS OF IONIZATION KINETICS IN LASER IRRADIATION

A. Velocity formula described by gaseous discharge theory

In this section, the propagation velocity of I-front is introduced in terms of the ionization kinetics in laser electric-field. To investigate the propagation of ionization wave, we considered one-dimensional propagation with a moving coordinate ($n_e = n_e(z-Ut)$), as presented in Fig. 8(a). T_e is assumed as uniform for simplicity. According to the streamer theory for the streamer head expansion in the electric field, the conservation of ne is expressed as,[20],[21]

$$\frac{dn_e}{dt} = \frac{\partial n_e}{\partial t} - U\frac{\partial n_e}{\partial z} = \nu_i n_e . \quad (2)$$

With the neglect of the time derivation term, Eq. (2) becomes $-U(\partial n_e/\partial z) = \nu_i n_e$. This partial differential equation is solvable via separation of variables. In the same manner as the streamer discharge, the velocity U is described by the relation between the time of avalanche ionization ν_i^{-1} and the distance l from the initial n_e to the n_e in the bulk plasma,

$$U = \frac{\nu_i l}{\ln(n_{e,l}/n_{e,0})} . \quad (3)$$

The electron density at distance l, $n_{e,l}$, was difficult to obtain in the experiment because the expected n_e is much lower than the detection limit of the spectrometer. Thus, $n_{e,l}$ was obtained from a function of the photon flux and the velocity, φ/U; then U is

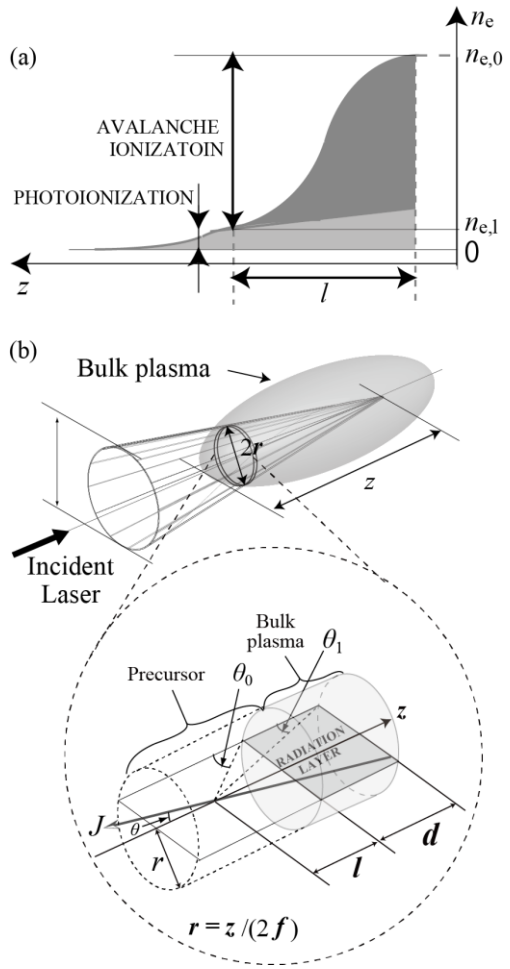

Fig. 8. (a) One-dimensional electron density distribution, (b) Schematic diagram explaining the calculation of the intensity of photon radiation which causes a wave to appear.

calculated as a solution to a system of equations. ν_i^{-1} can be obtained from the kinetics of electron in the laser electric field. When assuming that an electron which has an energy slightly greater than the ionization potential ε_i instantaneously ionizes an atom, the ionization frequency ν_i is definable using the time needed for ε ($= 3n_e k_B T_e/2$) to increase to ε_i, as,[7]

$$\nu_i = \left(\frac{d\varepsilon}{dt}\right)\frac{1}{\varepsilon_i}, \tag{4}$$

where ε_i of air (oxygen) and argon are 12.1 and 15.8 eV, respectively. The acquisition of laser energy via inverse bremsstrahlung at an average rate is described simply by the rate of change of electron energy $d\varepsilon/dt$,[17]

$$\frac{d\varepsilon}{dt} = \frac{e^2 E_0^2 \nu_m}{2m(\omega^2+\nu_m^2)} = 6.34\cdot 10^{13}\frac{\nu_m}{\omega^2+\nu_m^2}S \tag{5}$$

where e, E, m, and ω respectively denote the charge of an electron, the electric field related to laser intensity $S(z)$ using $E^2 = 4\pi S/c$,[7] the electron mass, and the angular frequency of the light. ν_m in air and argon are 2.99×10^{12} s^{-1} and 4.06×10^{12} s^{-1} at p = 101.3 kPa, respectively.[22] ω at λ = 10.6 and 1.05 μm are 1.78×10^{14} s^{-1} and 1.88×10^{15} s^{-1}, respectively. It is noteworthy that in micrometer-order laser irradiation, a multi-photon ionization rarely occurs because the 1 μm laser has photon energy of 1 eV that is much lower than ε_i.

Here the distance l and φ are functions of n_e, T_e, and λ, which can be estimated using spectroscopic results. The distance l was obtained in terms of the laser absorption by plasma,

$$l = \frac{4\pi}{c}\int_0^{1/k}\exp(-kz)\,dz\,. \tag{6}$$

The laser intensity S decreased along the laser axis caused by plasma absorption. This can be described by the semi-classical theory of laser absorption, which considers the interaction between electrons and heavy particles in the strong laser electric field, $dS/dz = -kS$. The net absorption coefficient, inverse Bremsstrahlung process, is determined as shown below.[23]

$$\begin{aligned} k &= k_{en} + k_{ei} \\ &= \frac{4}{3}\left(\frac{2\pi}{3m_e k_B T_e}\right)^{\frac{1}{2}}\frac{e^6\lambda^3 G\, n_e n_i}{hc^4 m_e}\left(\exp\left(\frac{hc}{\lambda k_B T_e}\right)-1\right) \\ &+ \frac{k_B T_e^{\,2} A(T_e)\lambda^3 n_e n_n}{hc}\left(1-\exp\left(\frac{hc}{\lambda k_B T_e}\right)\right) \end{aligned} \tag{7}$$

where $T_{ex} = T_e$ is valid in local thermal equilibrium plasma.

B. Photo-ionization by UV radiation from plasma

Recently, a preionization layer ahead of laser absorption layer was observed and reported in several papers. Koopman found the preionized layer using a ruby laser in a hydrogen background.[24] n_e in the precursor measured using a Langmuir probe and microwave diagnostics was less than 10^{17} m^{-3}. Diziere, using a GEKKO XII high-power solid state laser, found that a radiative precursor was driven ahead of the laser absorption wave.[25] Interferometry snapshots showed that n_e in the precursor was 10^{18} m^{-3}. These results suggest that seed electrons ahead of the laser-absorption wave were generated by photoionization from UV radiation of the laser-absorption wave.

UV radiation was estimated quantitatively using the obtained T_e and n_e behind the shock wave because a low degree of ionization in the preionized layer makes it difficult to observe the UV spectrum. The radiative transfer equation is,[26]

$$\frac{1}{c}\frac{\partial J_\nu}{\partial t} + \Omega\cdot\nabla J_\nu = \kappa(J_{\nu p} - J_\nu)\,, \tag{8}$$

where J_ν, $J_{\nu p}$, $\mathbf{\Omega}$, and κ respectively denote the radiation intensity, the equilibrium radiation intensity, the unit solid angle in the direction and the absorption coefficient. An important assumption is that the UV radiation intensity within the cross section of a cylindrical optical channel differs little from the value calculated for the channel axis, $J_\nu(\mathbf{\Omega}, x, r < R) \approx$

J_ν (**Ω**, x, 0**)**. In this case, the propagation direction **Ω** is characterized by angle θ between the vector **Ω** and the channel axis x; R is the radius of the beam, and $J_\nu(x, \mathbf{\Omega}) = J_\nu(x, \theta)$. The radiation-transport equation for the plane case can be presented in the form shown below. [26],[27]

$$\cos\theta \frac{\mathrm{d}J_\nu}{\mathrm{d}x} = \kappa(J_{\nu p} - J_\nu) \tag{9}$$

The mean-free path of photon-absorption λ_a is longer than that of free electron λ_e. In addition, λ_a ($\equiv (n_n\sigma)^{-1}$) is a function of the number density of neutral particles n_n and the cross section for photon-absorption σ. At room temperature and atmospheric pressure, n_n is estimated as 2.53×10^{25} m^{-3}. σ is 10^{-20} m^2 in photon energy ranging from 12.06 eV (= first ionization energy for O_2) to 200 eV. Therefore, λ_a is estimated as 10–100 μm.[27] However, the net cross-section of electron collisions is 10^{-18} – 10^{-19} m^2 in the same energy range as the photon above.[28] In fact, λ_e varies from 0.1 μm to 1.0 μm in the atmospheric pressure.[29] Consequently, photoionization is a dominant process in generating seed electrons ahead of the laser-absorption wave. λ_a in the bulk plasma is also much shorter than the thickness of preionized layer. In the range of $z > z_0$ and $z < z_0$, n_n was considered as 2.53×10^{25} and 1.20×10^{26} m^{-3} ,respectively, where z_0 is the boundary between the preionized layer and the bulk plasma.[10] Therefore, most of photons are re-absorbed by the bulk plasma. Consequently, the front of the bulk plasma only contributes the generation of seed electron at the head of preionized layer. From Eq. (9), the radiation intensity at point x on the axis of channel J (equal to the integral of j_ν in terms of frequency)[W/(m^{2}sterad.)] is [2]

$$J(x,\theta) = j_\nu \exp\left(-\frac{z}{\lambda_a\cos\theta}\right) \times \begin{cases} \dfrac{d}{\cos\theta}, & \left[0 < \theta < \theta_1 = \arctan\dfrac{r}{d+z}\right] \\ \left(\dfrac{r}{\sin\theta} - \dfrac{z}{\cos\theta}\right), & \left[\theta_1 < \theta < \theta_0 = \arctan\dfrac{r}{z}\right] \end{cases} \tag{10}$$

Here, j_ν [W/m^3] is the emissivity of the plasma, which is regarded as the photon-emitting layer because recombination or other energy loss mechanism occurs after absorption. r represents the radius of the I-front surface, which is determined by the displacement of the I-front, $r = 0.5\times$ (displacement of I-front)/(focusing f-number).[4] σ in air and argon are 10.0 and 2.92×10^{-21} m^2, respectively.[30],[31] Using the trapezoidal rule, numerical calculations were iterated 100 times. As z approaches infinity, the integration below the solid angle and the z-axis becomes convergent. Assuming that attenuation of the flux of thermal radiation is small in the radiating layer, the photon flux, φ_0, [photons/ (m^{2}s)] is equal to,[5]

$$\varphi_0 = \int_0^z \int_{\nu_i}^{\infty} \int_0^{\theta_0} \left(\frac{J}{h\nu_i}\right) \mathrm{d}z\, \mathrm{d}\nu\, \mathrm{d}\Omega\,. \tag{11}$$

Equation (11) can be integrated from ν_i to ∞ in terms of ν to evaluate the UV photons.

Radiation sources can be of three types: bound–bound, bound–free, and free–free transition radiation. The line radiation (bound–bound) is much less than continuum radiation (bound–free and free–free). Comparison of the relaxation time of electron–electron collision τ_{ee} and the decay time of line radiation from upper state q to the ground state, $\tau_{q,\mathrm{rad}}$, shows the following.[32]

$$\tau_{ee} = 0.3\times10^6 T_e^{3/2}/(n_e \ln\Lambda) \approx 10^{-14} \tag{12}$$

$$\tau_{q,\mathrm{rad}} = 6.2\times10^{-11} q^{4.5} Z^{-4} \le 10^{-9} \tag{13}$$

For example, the time of the hydrogen-like ion ($Z = 1$ and $q = 3$) is 10^{-9} s. For ($q > 3$), $\tau_{q,\mathrm{rad}}$ is longer than τ_{ee}, which means that the radiation of line spectral can be negligibly small. Consequently, a dominant spectral feature of high-density laser plasmas is the Bremsstrahlung (free–free) process. The total volumetric energy of the continuous plasma radiation in the frequency range of ν to $\nu + \mathrm{d}\nu$ per unit volume $j_\nu\,\mathrm{d}\nu$ can be expressed as shown below.[34]

$$j_\nu(\nu)\,\mathrm{d}\nu = 6.3\times10^{-53} \frac{Z^2 n_e n_i}{\sqrt{k_B T_e}} \exp\left(-\frac{h\nu}{k_B T_e}\right)\mathrm{d}\nu \tag{14}$$

Here, ν_i, and Z_{eff} respectively represent the ionization frequency and the nuclear effective charge. As presented in Fig. 8(b), the radiative layer d depth and the radius of the radiative surface are of the same order. In a cylindrical plane layer (finite thickness at spatially uniform temperature T_e and with an absorption coefficient).

C. Comparison of predicted and measured velocities

Predicted velocities U (symbols) compared with measured velocities u (solid line), which were obtained using a high-speed camera, are shown in Fig. 9 as a function of the laser intensity for the range of $S/S_{\mathrm{term}} = 0.65$–$1.75$. Table 1 shows the experimental parameters and, the measured and computed plasma-properties in order to obtain U. The displacement of the I-front was obtained from a sequence of images. u was deduced using a derivative of fitted curve. The most notable observation is that the agreement with u was fairly good and within the limits of expected error at varying laser intensities. Compared with different laser wavelengths, u at 10.6 μm laser was higher than that at 1 μm even if $n_{e,l}$ at 10.6 μm was much lower than at 1 μm. As evidenced by eq. (3), U depends strongly on the laser wavelength because the time of avalanche ionization is proportional to λ^2. The gaseous form dependency was unobserved because the ionization frequency ν_i depends slightly on the gaseous form, where the gaseous form only affects ν_m in the ionization frequency.

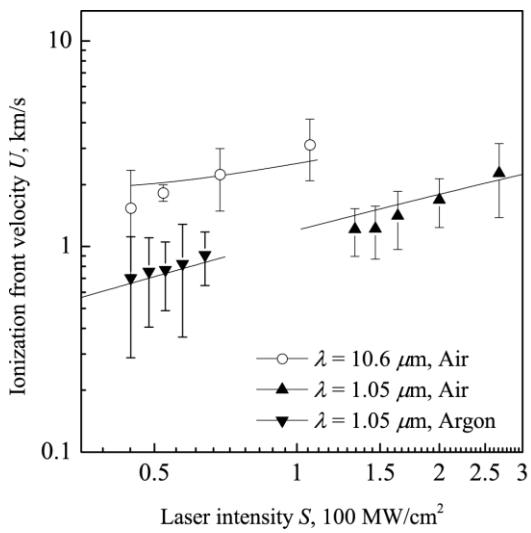

Fig. 9. Calculation and measurement results of U in terms of laser intensity S. All solid lines and symbols with error bars respectively represent the measured velocity obtained by laser-shadowgraph and laser intensity.

Our previous work suggested that the precursor ionization ahead of the shock wave regulates laser-absorption wave propagation.[10] This work quantitatively investigated how the ionization process affects the propagation mechanism. However, this model cannot address weak ionization in the precursor, and the interaction between radiation and low degree of ionization is a more complex mechanism. Laser-absorption waves are an extremely promising feature with many unclear mechanisms. Future numerical work must be done to investigate microscopic reactions including various ionized species.

V. Conclusion

The influences of laser-wavelength and gaseous form on laser-absorption wave propagation were investigated using a Nd:glass laser and a TEA CO_2 laser in argon and air atmospheres. u was measured using laser-shadowgraph and was estimated using a simple model consisting of the laser-absorption process with spectroscopic results. Results show that electron temperature and density can be estimated as 2–6 eV and (1.5–3.9) × 10^{24} m^{-3}, respectively, near the laser intensity threshold for laser-supported detonation. The evaluated velocities showed good agreement with the measurement velocities in all sets. These velocities were within the limits of expected error at varying laser intensities. U at longer wavelength is faster than that at shorter wavelength at the same laser intensity because the ionization frequency depends on the laser wavelength. Consequently, our model is useful to investigate how the states of plasma affect the advancement of ionization-wave front. This work quantitatively explained the propagation model of ionization wave using gaseous discharge physics.

References

[1] S. A. Ramsden, and P. Savic, "Radiative detonation model for development of laser-induced spark in air," *Nature,* vol. 203, no. 495, pp. 1217-&, 1964.

[2] Y. P. Raizer, "Breakdown and heating of gases under influence of a laser beam," *Soviet Physics Uspekhi-USSR,* vol. 8, no. 5, pp. 650-&, 1966.

[3] L. J. Radziemski, and D. A. Cremers, *Laser-Induced Plasmas and Applications*, New York: CRC Press, 1989.

Table 1. Experimental parameters and measured plasma propertie

Experimental parameters			
Laser wavelength: λ_{LASER}, μm	1.053	1.053	10.6
Ambient gaseous form	Argon	Air	Air
Laser intensity: S, MW/cm^2	(3.8-6.7)×10^1	(1.3-2.8)×10^2	(4.0-10.9)×10^1
LSD termination: S_{term}, MW/cm^2	4.9×10^1	1.7×10^2	6.9×10^1
Bulk Plasma parameters			
Electron density: n_e, 10^{24} m^{-3}	3.0-3.9	2.6-3.3	1.5-2.6
Electron density:T_e, 10^4 K	3.7-4.1	5.3-6.1	2.5-2.6
Cross-sectional area of Photoabsorption: σ, 10^{-21} m^2	2.92	10.0 (O_2)	
Ionization threshold: $h\nu_i$, eV	15.8	12.1 (for O_2)	
Parameters estimated from measured n_e and T_e			
optical depth: l, mm	2-3	4-5	0.2-0.3
Electron density: $n_{e,l}$, m^{-3}	(5.8-13.7)×10^{17}	(3.8-5.6)×10^{18}	(4.8-30.2)×10^{15}

[4] K. Mori, K. Komurasaki, and Y. Arakawa, "Influence of the focusing F number on the heating regime transition in laser absorption waves," *J. Appl. Phys.,* vol. 92, no. 10, pp. 5663-5667, 2002.

[5] K. Mori, K. Komurasaki, and Y. Arakawa, "Energy transfer from a laser pulse to a blast wave in reduced-pressure air atmospheres," *J. Appl. Phys.,* vol. 95, no. 11, pp. 5979-5983, 2004.

[6] K. Mori, K. Komurasaki, and Y. Arakawa, "Threshold laser power density for regime transition of a laser absorption wave in a reduced-density air atmosphere," *Appl. Phys. Lett.,* vol. 88, no. 12, pp. 3, Mar, 2006.

[7] Y. P. Raizer, *Laser-Induced Discharge Phenomena*, New York: Springer, 1978.

[8] P. Bournot, P. A. Pincosy, G. Inglesakis, M. Autric, D. Dufresne, and J. P. Caressa, "Propagation of a laser-supported detonation-wave," *Acta Astronautica,* vol. 6, no. 3-4, 1979, 1979.

[9] W. E. Maher, R. B. Hall, and R. R. Johnson, "Experimental study of ignition and propagation of laser-supported detonation-waves," *J. Appl. Phys.,* vol. 45, no. 5, 1974, 1974.

[10] K. Shimamura, K. Hatai, K. Kawamura, A. Fukui, A. Fukuda, B. Wang, T. Yamaguchi, K. Komurasaki, and Y. Arakawa, "Internal structure of laser supported detonation waves by two-wavelength Mach–Zehnder interferometer," *J. Appl. Phys.,* vol. 109, no. 8, 2011.

[11] Y. Hidaka, E. M. Choi, I. Mastovsky, M. A. Shapiro, J. R. Sirigiri, and R. J. Temkin, IEEE Trans. Plasma Sci., vol. 36, no. 4, pp. 936, Aug., 2008.

[12] B. Chaudhury and J. P. Boeuf, "Computational Studies of Filamentary Pattern Formation in a High Power Microwave Breakdown Generated Air Plasma," IEEE Trans. Plasma Sci, vol. 38, no. 9, Sep., 2010.

[13] Y. P. Raizer, *Gas Discharge Physics*, New York: Springer, 1991.

[14] B. Wang, K. Komurasaki, T. Yamaguchi, K. Shimamura, and Y. Arakawa, "Energy conversion in a glass-laser-induced blast wave in air," *J. Appl. Phys.,* vol. 108, no. 12, Dec, 2010.

[15] A. De Giacomo, R. Gaudiuso, M. Dell'Aglio, and A. Santagata, "The role of continuum radiation in laser induced plasma spectroscopy," *Spectrochimica Acta Part B – Atomic Spectroscopy,* vol. 65, no. 5, pp. 385-394, May, 2010.

[16] G. K. Wertheim, M. A. Butler, K. W. West, and D. N. Buchanan, "Determination of Gaussian and Lorentzian content of experimental line-shapes," *Rev. Sci. Inst.,* vol. 45, no. 11, pp. 1369-1371, 1974.

[17] G. Bekefi, *Principles of Laser Plasmas,* New York, Wiley-Interscience, 1976.

[18] H. R. Griem, *Plasma Spectroscopy*, New York, McGraw-Hill, 1964).

[19] (Online). NIST Atomic Spectra Database, http://physics.nist.gov.

[20] A. A. Kulikovsky, "Analytical model of positive streamer in weak field in air: Application to plasma chemical calculations," *IEEE Trans. Plasma Sci.*, vol. 26, no. 4, pp. 1339-1346, Aug, 1998.

[21] E. M. Bazelyan, Y. P. Raizer, *Spark Discharge*, New York: CRC-Press, 1997.

[22] A. D. MacDonald, *Microwave Breakdown in gases*, New York: Wiley, 1966.

[23] N. H. Kemp and P. F. Lewis, Laser-heated thruster, NASA Report No. CR-161665, 1980.

[24] D. W. Koopman, "Precursor ionization fronts ahead of expanding laser-plasmas," *Physics of Fluids,* vol. 15, no. 1, pp. 56-&, 1972.

[25] A. Diziere, C. Michaut, M. Koenig, C. D. Gregory, A. Ravasio, Y. Sakawa, Y. Kuramitsu, T. Morita, T. Ide, H. Tanji, H. Takabe, P. Barroso, and J. M. Boudenne, "Highly radiative shock experiments driven by GEKKO XII," *Astro. Space Sci.,* vol. 336, no. 1, pp. 213-218, Nov, 2011.

[26] Y. B. Zel'dovich, and Y. P. Raizer, *Physics of Shock Waves and High-Temperature Hydrodynamic Phenomena*, New York: Courier Dover Publications, 2002.

[27] V. I. Fisher, "On the fast gas ionization wave in an intense laser-beam," *Zhurnal Eksperimentalnoi I Teoreticheskoi Fiziki,* vol. 79, no. 6, pp. 2142-2151, 1980.

[28] B. L. Henke, E. M. Gullikson, and J. C. Davis, "X-ray interactions - photoabsorption, scattering, transmission, and reflection at E=50-30,000 EV, Z=1-92," *Atomic Data and Nuclear Data Tables,* vol. 54, no. 2, pp. 181-342, 1993.

[29] Y. Itikawa, "Cross sections for electron collisions with nitrogen molecules," *J. Phys. Chem. Ref. Data,* vol. 35, no. 1, pp. 31-53, Mar, 2006.

[30] G. V. Marr and J. B. West, "Absolute photoionization cross-section tables for helium, neon, argon, and krypton in the VUV spectral regions," *Atomic Data and Nuclear Data Tables*, vol. 18, no. 5, pp. 497-508, 1976.

[31] G. R. Cook, and P. H. Metzger, "Photoionization + absorption cross sections of O2 + N2 in 600- to 100-A REGION," *Journal of Chemical Physics,* vol. 41, no. 2, pp. 321-336, 1964.

[32] R. Wilson, "The spectroscopy of non-thermal plasmas," *J. Quantitative Spectroscopy & Radiative Transfer,* vol. 2, no. 4, 1962, 1962.

[33] L. Spitzer, *Physics of Fully Ionized Gases*, New York: John Wiley & Sons Inc., 1962.

[34] T. K. Bose, *High Temperature Gas Dynamics*, New York: Springer, 1979.

Kohei Shimamura (M'11) received the B.S. degree of engineering from Keio University, Yokohama, Japan, in 2009 and the M.S. and Ph.D. degrees of science from the University of Tokyo, Chiba, Japan, in 2011 and 2014, respectively.

In 2013, he worked as a research fellow of the Japan Society for the Promotion of Science. Since 2014, he has been an Assistant Professor with the Department of Engineering Mechanics and Energy, University of Tsukuba, Japan.

Kimiya Komurasaki received the B.S., M.S. and Ph.D. degrees from The University of Tokyo, Tokyo, Japan, in 1987, 1989 and 1992, respectively.

Since 2009, he has been a Professor in the Department of Advance Energy and in the Department of Aeronautics and Astronautics, The University of Tokyo.

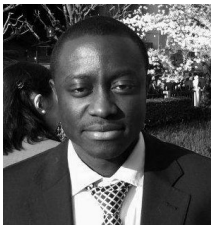

Joseph A. Ofosu (M'12) received the B.S. degree from The Kwame Nkrumah University of Science and Technology, Ghana in 2007 and the M.S. degree from The University of Tokyo in 2012.

He is currently a Ph.D. candidate of The University of Tokyo.

Hiroyuki Koizumi received the B.S. degree from Keio University, Yokohama, Japan, in 2000 and the M.S. and Ph.D. degrees from The University of Tokyo, Tokyo, Japan, in 2002 and 2006, respectively.

Since 2011, he has been an Associate Professor in the Research Center for Advanced Science and Technology and in the Department of Aeronautics and Astronautics, The University of Tokyo.